Earth and Planetary Science Letters 462 (2017) 99–109

Contents lists available at ScienceDirect

Earth and Planetary Science Letters

www.elsevier.com/locate/epsl

The evolution of pore connectivity in volcanic rocks

Mathieu Colombier [a,*], Fabian B. Wadsworth [a], Lucia Gurioli [b], Bettina Scheu [a], Ulrich Kueppers [a], Andrea Di Muro [c], Donald B. Dingwell [a]

[a] Department of Earth and Environmental Sciences, Ludwig-Maximilians-Universität München, Germany
[b] Université Clermont Auvergne, CNRS, IRD, OPGC, Laboratoire Magmas et Volcans, F-63000 Clermont-Ferrand, France
[c] Institut de Physique du Globe de Paris, Observatoire Volcanologique du Piton de la Fournaise (OVPF), Sorbonne Paris Cité, UMR 7154 CNRS, Université Paris Diderot, France

ARTICLE INFO

Article history:
Received 24 June 2016
Received in revised form 10 January 2017
Accepted 15 January 2017
Available online 30 January 2017
Editor: T.A. Mather

Keywords:
connectivity
permeability
percolation threshold
eruptive style
vesiculation
densification

ABSTRACT

Pore connectivity is a measure of the fraction of pore space (vesicles, voids or cracks) in a material that is interconnected on the system length scale. Pore connectivity is fundamentally related to permeability, which has been shown to control magma outgassing and the explosive potential of magma during ascent in the shallowest part of the crust. Here, we compile a database of connectivity and porosity from published sources and supplement this with additional measurements, using natural volcanic rocks produced in a broad range of eruptive styles and with a range of bulk composition. The database comprises 2715 pairs of connectivity C and porosity ϕ values for rocks from 35 volcanoes as well as 116 products of experimental work. For 535 volcanic rock samples, the permeability k was also measured. Data from experimental studies constrain the general features of the relationship between C and ϕ associated with both vesiculation and densification processes, which can then be used to interpret natural data. To a first order, we show that a suite of rocks originating from effusive eruptive behaviour can be distinguished from rocks originating from explosive eruptive behaviour using C and ϕ. We observe that on this basis, a particularly clear distinction can be made between scoria formed in fire-fountains and that formed in Strombolian activity. With increasing ϕ, the onset of connectivity occurs at the percolation threshold ϕ_c which in turn can be hugely variable. We demonstrate that C is an excellent metric for constraining ϕ_c in suites of porous rocks formed in a common process and discuss the range of ϕ_c values recorded in volcanic rocks. The percolation threshold is key to understanding the onset of permeability, outgassing and compaction in shallow magmas. We show that this threshold is dramatically different in rocks formed during densification processes than in rocks formed in vesiculating processes and propose that this value is the biggest factor in controlling the evolution of permeability at porosities above ϕ_c.

1. Introduction

Volcanic eruption style is controlled dominantly by the efficiency with which exsolved volatiles can outgas from the system at shallow levels (e.g., Rust and Cashman, 2004; Gonnermann and Manga, 2012). This is governed by the development and longevity of permeability (e.g., Blower, 2001). The explosive potential, driven by a pressurizing gas phase, can be reduced if permeability is quickly established and remains high (e.g., Eichelberger et al., 1986; Klug and Cashman, 1996). Understanding the time-dependence of permeability evolution in shallow magmatic systems should help to refine models of a wide range of magmatic processes, including heat transfer (e.g., Connor et al., 1997), volcanic welding (e.g., Wadsworth et al., 2014; Heap et al., 2015), fragmentation likelihood (e.g. Mueller et al., 2008) and volcanic gas flux (e.g., of SO_2; Edmonds and Herd, 2007). In all these cases, the evolution of gas permeability is strongly coupled to the evolution of the bulk porosity of the system by constitutive laws that depend on the geometry of the pore space (e.g., Saar and Manga, 1999; Blower, 2001; Wadsworth et al., 2016a, 2016b). Metrics for the geometry of pore space, including inter-pore aperture size, pore network anisotropy and tortuosity or, in the case of a welding scenario, initial particle size and shape, have all been found to be useful in scaling models of permeability with porosity (e.g., Blower, 2001; Le Pennec et al., 2001; Bernard et al., 2007; Yokoyama and Takeuchi, 2009; Wright et al., 2009; Degruyter et al., 2010; Wright and Cashman, 2014; Wadsworth et al., 2016a, 2016b).

* Corresponding author.
E-mail address: mathieu.colombier@min.uni-muenchen.de (M. Colombier).

http://dx.doi.org/10.1016/j.epsl.2017.01.011

Pore connectivity, the fraction of total porosity that is connected, directly records the onset of permeability (e.g., Rust and Cashman, 2011). These two properties, connectivity and permeability, are different since permeability is a vector quantity and is dependent on several pore properties such as tortuosity and anisotropy whereas connectivity is a scalar quantity and is only a function of the extent of coalescence or crack size and number density in the system. Connectivity is thus a relatively accessible variable as it does not require quantification of anisotropy in order to be obtained.

In the simplest view of magma ascent, volatiles exsolve from the melt, and lead to bubble nucleation, growth and coalescence (e.g., Gonnermann and Manga, 2007). At a critical percolation porosity (the percolation threshold ϕ_c), bubble coalescence becomes system-spanning leading to the development of connectivity (e.g. Blower, 2001). In volcanic rocks, porosity is often composed dominantly or even completely of connected porosity (i.e., isolated porosity of zero) reflecting extensive coalescence or microcracking (e.g., Robert et al., 2008; Kennedy et al., 2010). If continued volatile exsolution into this coalescing pore network is sufficiently vigorous, or ascent is sufficiently rapid, then the gas pressure rises and can result in fragmentation (e.g., Namiki and Manga, 2008).

The traditional view espoused above is ubiquitously cast as a system in which porosity, and connectivity increase during ascent until fragmentation. However, a more nuanced view acknowledges that magma with a highly connected pore phase is unstable if the gas pressure does not balance the magmastatic pressure. This can be the case when connectivity extends over large length-scales where the pore pressure can drop due to outgassing through the system. Magmas for which this is the case will densify either by compaction (Michaut et al., 2009) or by surface tension at melt–gas interfaces (Wadsworth et al., 2014, 2016a; Kennedy et al., 2016), decreasing porosity back toward a threshold ϕ_c.

In addition to nucleating and growing bubbles, magma porosity can be formed by cracks (e.g. Lavallée et al., 2008) or by crack-filling granular magma such as tuffisite (e.g. Kendrick et al., 2016) that possibly represents intra-conduit fragmentation events in the absence of explosive eruption (e.g. Gonnermann and Manga, 2003; Castro et al., 2012). In the case of cracks, connectivity can be increased rapidly with little change in porosity. Crack development is ubiquitous in shallow dome-forming lavas (e.g., Calder et al., 2015). In the case of the formation of granular materials, the inter-particle connectivity is typically high (Wadsworth et al., 2016a).

We have collated literature data in order to explore a connectivity metric for porosity that has been used to elucidate the development of permeability (Farquharson et al., 2015). We show that while vesiculation will increase porosity ϕ and increase connectivity at $\phi > \phi_c$ (e.g., Blower, 2001), crack-closure, viscous compaction of bubbly magma, gas-resorption, and volcanic welding all conspire to decrease porosity and connectivity toward a low ϕ_c. We highlight that the ϕ_c intercepted during porosity increase need not be the same value as that which is intersected during porosity-decreasing processes. This is inherent in the concept of a permeability hysteresis (Rust and Cashman, 2004; Michaut et al., 2009). We propose that pore-connectivity is useful for distinguishing global composition-dependent characteristics of magma porosity development and destruction and we explore the efficacy of this metric for understanding the evolution of eruption style.

2. Methodology

2.1. Definitions and measuring techniques

In most previous studies dealing with the evolution of pore connectivity with porosity, the results have been presented by visualizing the connected porosity ϕ' as a function of the bulk porosity ϕ (Klug et al., 2002; Formenti and Druitt, 2003; Bouvet de Maisonneuve et al., 2009; Shea et al., 2012). The interpretation of such correlation plots is difficult because the trends are not easy to discriminate and interpret when data plot close to the equiline. A more intuitive way to make use of these results is to plot pore connectivity as a function of bulk porosity, an approach that has been adopted in only very few studies to date (Shimano and Nakada, 2006; Nakamura et al., 2008; Okumura et al., 2013; Farquharson et al., 2015; Colombier et al., 2017). We use the common definition of connectivity C where

$$C = \frac{\phi'}{\phi} \tag{1}$$

In this study, and in the case of ~99% of the values in the database here compiled, we measure ϕ' by a pycnometry method. With this technique, pore clusters connected to the exterior of a rock sample are considered connected porosity. However, these pores do not necessarily contribute to fluid transport and permeability. A subset of the data represent a ϕ' determined using water impregnation (Kato, 1987; Nakamura et al., 2008) or by X-ray tomographic imaging techniques (Okumura et al., 2008; Song et al., 2001). The pore connectivity can also be qualitatively estimated from the Euler characteristic which is calculated by counting the numbers of connections and isolated objects (Vogel, 2002). Finally, it can also be retrieved using skeleton analysis which relies on the quantification of number and geometry of the disconnected pore medial axis (Lindquist et al., 1996). While these different definitions of connectivity yield similar results and are used synonymously in this study, some discrepancies are likely and should be considered.

2.2. Compilation of the connectivity database

We compiled a large database of porosity and connectivity comprising bulk-rock composition and measurement techniques for natural and experimental data from studies published in the last 30 years as well as unpublished data for erupted volcanic materials measured herein. The compiled database results in 2715 pairs of connectivity and porosity values for natural volcanic rocks across 35 volcanoes covering a broad range of eruptive styles and compositions and 116 pairs from 7 experimental studies. This database includes rhyolitic (Kato, 1987; Klug et al., 2002; Rust and Cashman, 2004; Mueller, 2007; Nakamura et al., 2008; Bouvet de Maisonneuve et al., 2009; Alfano et al., 2012; Nguyen et al., 2014), dacitic (Rust et al., 1999; Mueller, 2007; Wright et al., 2007; Nguyen et al., 2014; Heap et al., 2015), phonolitic and trachytic (Shea et al., 2012; Colombier et al., 2017), andesitic (Formenti and Druitt, 2003; Mueller, 2007; Platz et al., 2007; Bernard et al., 2007; Giachetti et al., 2010; Farquharson et al., 2015), and basaltic to basaltic andesitic (Rust et al., 1999; Song et al., 2001; Mueller, 2007; Kawabata et al., 2015) volcanic rocks from a wide range of sites, as well as naturally welded deposits (Klug et al., 2002; Michol et al., 2008; Wright and Cashman, 2014; Heap et al., 2015). It should be noted that more than 90% of the data for the trachytes arise from analysis of rocks of a single eruption (Colombier et al., 2017). The database also comprises experimental products from both vesiculation (Okumura et al., 2008; Takeuchi et al., 2009) and densification experiments (Robert et al., 2008; Okumura et al., 2013; Vasseur et al., 2013; Kennedy et al., 2016; Vasseur et al., 2016).

We complement the above database with unpublished measurements of basaltic scoria from the Chisny AD 381 BP (Morandi et al., 2016) lava fountaining eruption (Piton de la Fournaise; DynVolc database), Stromboli 2011 and 2013 eruptions (DynVolc

database), and of andesitic pumices from Montagne Pelée volcano. Where measurements were made by the authors, helium-pycnometers at LMU (Ludwig-Maximilians-Universität) and LMV (Laboratoire Magmas et Volcans) were used (Quantachrome Ultrapyc 1200e and Micromeritics Accupyc 1340, respectively). In the supplementary file, we provide Supplementary Table 1 with a list of all the contributions to the database specifying the publication title, the eruption date and style or the type of experimental study, the number of samples analyzed, the technique used to measure connectivity, the porosity and connectivity ranges and, if available, the sample permeability range. We also provide the complete database (Supplementary Table 2) with porosity, connectivity and if available permeability data for each dataset, as well as the sample type, chemistry, eruption and eruptive style associated for natural volcanic rocks or the type of experiments for experimental data.

2.3. Potential weaknesses in the connectivity database

The database includes data with $C > 1$. Since such connectivity values above unity are unphysical, we have to consider the potential sources of errors on the measurements. Key to the accurate measurement of total porosity is knowledge of the density of the solid, pore-free phase(s) in the volcanic rock. A first weakness in the data compiled here arises from the value chosen for the solid density in the calculation of the porosity. Indeed, in some studies only the solid-density of one representative clast is measured and this density value is used to compute total porosity for a suite of samples. This carries with it the implicit assumption that the solid density does not vary from clast-to-clast. However, heterogeneity in the phenocryst assemblage between clasts or variations in bulk composition may be common. This can lead to unphysical connectivity values greater than 1. To address this issue, Wright and Cashman (2014) demonstrate that a range of solid density could be plausible for welded deposits and discuss difference that may arise due to chemical variations. However, in most studies the rock population studied are more homogeneous with little variations of the solid density. This was the case for example for a breadcrust bomb population from Soufrière Hills volcano (Giachetti et al., 2010) and welded block and ash flows deposits from Mount Meager volcano (Michol et al., 2008) in which the solid density of a large number of rocks were measured and showed very small standard deviation. In this case, the potential source of error on connectivity arises only from determination of both bulk and connected porosities. In a few studies, these errors are quoted by the authors and allow us to determine the error on connectivity (Formenti and Druitt, 2003; Michol et al., 2008; Giachetti et al., 2010; Shea et al., 2012).

Another drawback to consider is that the connectivity that is measurable on typically-sized rock sample (typically on the order of $\sim 10^{-5}$ to 10^{-7} m^3) may not scale to volcanic length-scales. That is, connectivity of pore networks extends over finite lengths and porosity that is system spanning in the laboratory may not be system spanning in nature. Nevertheless, these measurements remain informative when interpreting laboratory-scale permeability measurements on which most permeability scaling laws are based.

3. Results

Connectivity C co-varies with ϕ in a trend that depend on the process involved in controlling changes in ϕ. In what follows, we present subsets of the compiled database to analyze these trends for (1) experimental or natural data for which the mechanism by which connectivity was created or destroyed is known, and then (2) data from natural rocks of a wide range of bulk chemistry. By adopting this two-stage analysis we aim to discriminate trends that can inform us about the processes by which connectivity is typically established or destroyed in magmas that come to be deposited as volcanic rocks.

3.1. Contrasting vesiculation and densification trends

Here we constrain the trends in which ϕ was an increasing function of time in experiments in which samples were vesiculated to different total ϕ. In these experimental data, the onset of non-zero C occurred at ϕ_c, which is the point at which bubble coalescence spanned the measured sample or connected to the outside. We term these trends "vesiculating" to refer to any trend in which bubble nucleation, growth, coalescence and forced gas percolation, or all of these dominate the mechanism by which ϕ increases. We distinguish vesiculating trends from those in which experimental work showed that ϕ decreased with time, which we term "densifying".

Fig. 1a shows the relationship between C and ϕ for vesiculating trends for a range of materials. First, the post-experimental results are shown for samples formed in vesiculation experiments (Okumura et al., 2008; Takeuchi et al., 2009) performed with and without syn-vesiculation shear stress imposed on the samples. In the former case, a qualitative estimate of the minimum threshold ϕ_c is $\sim$0.21, whereas in the latter case, $0.42 < \phi_c < 0.6$. These experiments confirm that for the vesiculating trend, the positive correlation of C with ϕ can be used to estimate a wide range of ϕ_c which will be discussed later (see Section 4.2).

We compare the experimental results with those from samples for which ϕ is known to have been a positive function of time. Breadcrust bomb samples from Soufrière Hills (Giachetti et al., 2010), Unzen (Mueller, 2007) and Guagua Pichincha (Wright et al., 2007) volcanoes are shown. These trends are characterized by post-fragmentation vesiculation of the bomb-cores while the bomb-rinds remained less porous due to fast quenching and solidification. As a result, the rinds record $0 \leq \phi \leq 0.25$ and the vesicles inside are completely isolated with $C = 0$, whereas their associated cores record higher porosity $0.2 \leq \phi \leq 0.7$ and corresponding $0.65 \leq C \leq 0.95$. Note that in the case of Unzen and Guagua Pichincha volcanoes (Mueller, 2007; Wright et al., 2007) the rinds were not measured. The ϕ_c at which connectivity onset can be estimated is likely to be in the range of the porosity of the rinds, that is $0 \leq \phi_c \leq 0.25$. Finally, we compare these data with rhyolitic pumices that contain vesicles with no diagnostic sign of shear-deformation or post-vesiculation collapse and which are reported to record coalescence features (Klug et al., 2002; Mueller, 2007; Bouvet de Maisonneuve et al., 2009; Nguyen et al., 2014). These pumices show a wide range of C from 0.25 to $\sim$1 over a small range of porosity $0.63 \leq \phi \leq 0.85$. Qualitative estimates of what the value of ϕ would be at $C = 0$, might suggest a high ϕ_c of >0.5.

Fig. 1b shows data from natural volcanic rocks that can be interpreted to be the result of densification mechanisms in what was initially a granular material and evolved to be non-granular and dense (Klug et al., 2002; Michol et al., 2008; Wright and Cashman, 2014; Heap et al., 2015) and experimental data from densifying systems (Robert et al., 2008; Okumura et al., 2013; Vasseur et al., 2013, 2016; Kennedy et al., 2016). The compaction experiments from Robert et al. (2008) and the sintering experiments from Vasseur et al. (2013, 2016) were performed using initially granular materials. Robert et al. (2008) used a rhyolitic volcanic ash with a high initial porosity ($\phi_i \approx 0.8$) as starting material, whereas Vasseur et al. (2013, 2016) used angular glass fragments with an initial porosity of $\phi_i \approx 0.4$. In these experiments ϕ decreased with time while the material maintained a high connectivity around $C \sim 1$. Only at the late stages of compaction or sintering, with continued densification did C decrease toward a low ϕ_c that can be qualitatively assessed to be on the

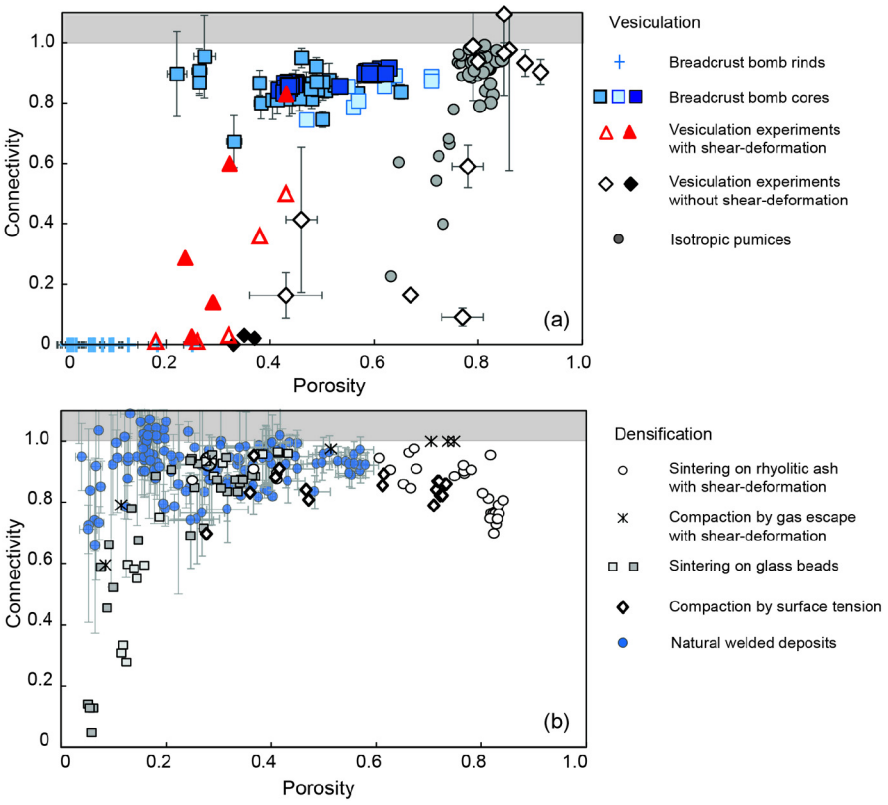

Fig. 1. The covariance of C with ϕ for systems that are dominantly recording (a) vesiculation and (b) densification. In (a) we show natural data from samples of breadcrust bomb rinds (blue crosses; Giachetti et al., 2010) and breadcrust bomb cores (blue squares; Mueller, 2007; Wright et al., 2007; Giachetti et al., 2010) from Soufrière Hills volcano, Guagua Pichincha volcano and Unzen volcano as well as natural pumice data for which there is no sign of shear deformation (grey circles; Klug et al., 2002; Mueller, 2007; Bouvet de Maisonneuve et al., 2009; Nguyen et al., 2014). Additionally we give results of vesiculation experiments with shear stresses applied during vesiculation (red triangles; Okumura et al., 2008) and without shear stresses (black and white diamonds; Okumura et al., 2008; Takeuchi et al., 2009). (b) We show the results of densification experiments consisting of sintering of glass beads (grey squares; Vasseur et al., 2013, 2016), compaction of sintered rhyolitic ash (black open circles; Robert et al., 2008) and compaction of rhyolitic melt by gas escape (black crosses; Okumura et al., 2013). We additionally show data from natural samples from welded deposits (blue circles; Klug et al., 2002; Michol et al., 2008; Wright and Cashman, 2014; Heap et al., 2015). The grey fields correspond to unphysical values of connectivity with $C > 1$. When quoted in the original study, the uncertainties on connectivity and porosity are represented. (For interpretation of the references to colour in this figure legend, the reader is referred to the web version of this article.)

order of $\phi_c \approx 0.05$. The experimental results of Okumura et al. (2013) demonstrate a similar evolution of ϕ and C down to a similar ϕ_c. However, in this study (Okumura et al., 2013) the compaction was a result of gas escape after an initial vesiculation and coalescence process. In Kennedy et al. (2016), the densification was a consequence of surface tension processes and also led to a decrease of C with ϕ. The natural datasets selected to demonstrate the densification trend are those from the Wineglass Tuff (Crater Lake; Klug et al., 2002), welded block and ash flow deposits (Mount Meager volcano; Michol et al., 2008; Heap et al., 2015), and the Shevlin Park Tuff (Wright and Cashman, 2014). We see that these natural datasets follow a similar relationship between ϕ and C as the experimental densification trend with a dramatic drop of porosity and a less pronounced and more scattered decrease of connectivity.

3.2. Trends associated with bulk composition

In Fig. 2 we present compiled datasets for natural volcanic rocks grouped by bulk chemical composition. Further distinction is made between vesicular rocks erupted during explosive activity (pumice or scoria and breadcrust bombs) and volcanic rocks derived from effusive eruptions such as lavas, dome lavas sampled *in situ* or in block and ash flow deposits where these distinctions are made in the studies originating the data and not here. Some problems with this simple separation might be encountered with transitional or complex eruption styles. For the rocks from explosive basaltic eruptions, we further differentiate between those from Strombolian eruptions and those from Hawaiian fire fountain activity.

The first observation we make is that C is high for most volcanic rocks independent of eruptive style. A broad range of connectivity is nevertheless observed for rhyolitic pumices and basaltic scoria (Figs. 2a and b). We emphasize that similar patterns can be discerned across all compositions; namely that rocks formed in explosive eruptions tend to have a relationship between C and ϕ that is distinct from rocks formed in effusive activity. Due to the high C in all rocks, it is difficult to discern what ϕ_c is for each rock type except for the rinds of the breadcrust bombs (Fig. 1). However, it is clear that the minimum ϕ for rocks formed in explosive activity is greater than the minimum ϕ found for rocks formed in effusive activity. The dacitic, andesitic and trachytic rocks formed by effusive activity record low-ϕ trends that show how C is an increasing function of ϕ.

Another feature is that the scoria from Hawaiian fire fountaining and from Strombolian activity have a similar range of porosity but the former have a much broader range of connectivity and at lower average values.

The global trends recorded in Fig. 2 are less diagnostic of the mechanism of formation, than the targeted and experimental data presented in Fig. 1.

3.3. Connectivity and permeability

The onset of system-spanning connectivity at ϕ_c is the onset of non-zero permeability k. The variable C does not include infor-

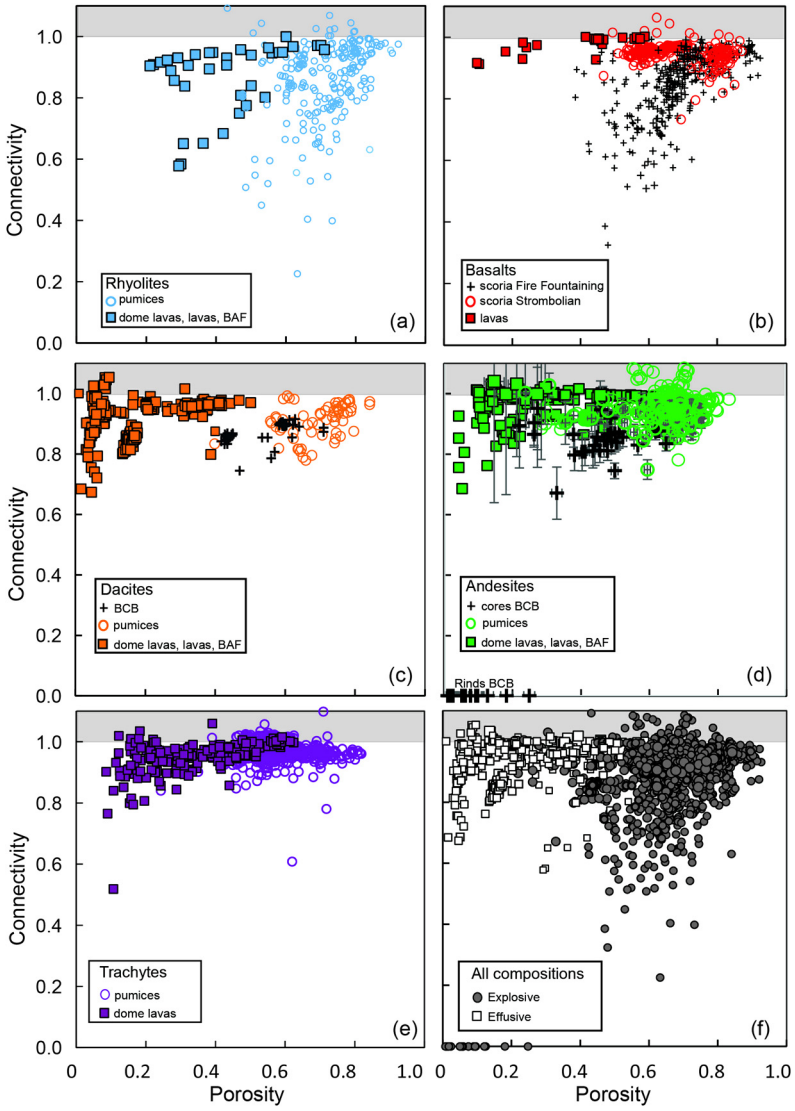

Fig. 2. The covariance of C with ϕ for all natural rocks classified by bulk rock composition. (a) Rhyolites differentiated into pumices (blue open circles) and effusive rocks (blue squares). (b) Basalts divided into scoria that are formed in fire fountain activity (black cross), scoria formed in Strombolian activity (red open circles) and lavas (red squares). (c) Dacites divided into pumices (orange open circles), breadcrust bombs (black cross) and effusive rocks from domes, lavas or block and ash flow deposits (orange squares). (d) Andesites divided into pumices (green open circles), breadcrust bomb cores and rinds (black cross) and effusive rocks from domes, lavas and block and ash flows (green squares). (e) Trachytes divided into pumices (purple open circles) or dome rocks (purple squares). (f) All data coarsely separated into rocks formed during explosive eruptions (grey circles) and rocks formed by effusive eruptions (black open squares). BCB and BAF are breadcrust bombs and rocks from block and ash flow deposits, respectively. The grey fields correspond to unphysical values of connectivity with $C > 1$. Details on compiled data are available in Supplementary Table 2. When quoted in the original study, the uncertainties on connectivity and porosity are represented. (For interpretation of the references to colour in this figure legend, the reader is referred to the web version of this article.)

mation about anisotropy. Furthermore, k depends strongly on pore aperture size and tortuosity (e.g. Blower, 2001; Saar and Manga, 1999) whilst C does not. Therefore, typically, only the variation of k with ϕ are constrained and not the variations of C with ϕ. Notably, as shown in Figs. 1 and 2, for most vesiculating systems, there is an extended region of $\phi > \phi_c$ where $0 < C < 1$, demonstrating that using a bulk metric ϕ includes pores that are isolated and not contributing to permeable flow which confuses interpretations of model constraints. To solve this issue, often only the connected porosity is used when exploring relationships with permeability (Wright et al., 2009; Farquharson et al., 2015).

We compare in this section the evolution of connectivity and permeability with porosity to assess if, despite these discrepancies, these properties still provide similar information about the vesiculation and densification processes. For 535 volcanic rock samples, parameters k, ϕ and C are available. Fig. 3 shows how a plot of the covariance of C and ϕ compares with the more typical k–ϕ plot for the same datasets.

Rocks produced in effusive events record similar characteristics using either metric C or k (Figs. 3a and b). Two key features are (1) the steep increase of connectivity and permeability with porosity up to a porosity threshold of around 0.2 for andesites and dacites and (2) the lower connectivity and permeability for rhyolites at a given porosity compared to less evolved rocks produced in effusive events.

Vesicular rocks produced in explosive events (pumice, breadcrust bombs and scoria) also show similar patterns when either C or k are compared relative to ϕ (Figs. 3c and d). In both cases, the andesites and trachytic pumices and the basaltic scoria plot at a higher C and k at a given ϕ than dacitic and rhyolitic breadcrust bombs and pumices. However, when only considering k, all dacitic and rhyolitic breadcrust bombs and pumices cluster ap-

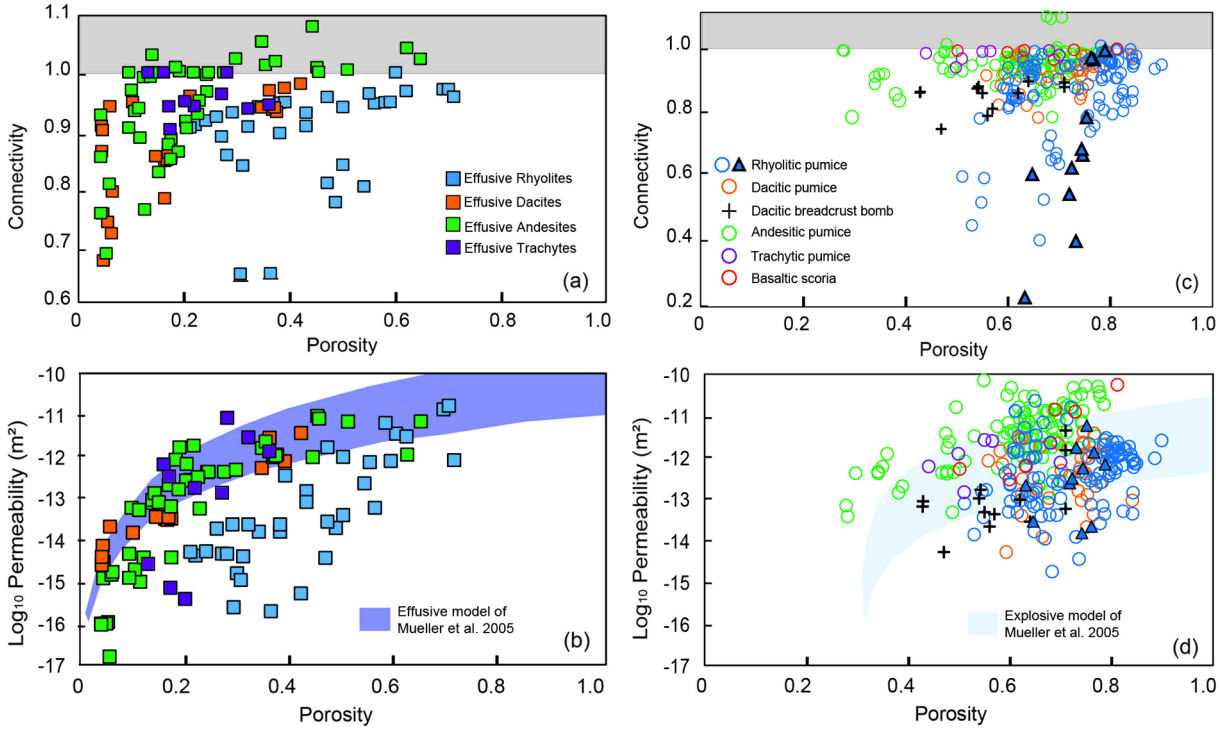

Fig. 3. Comparison between the evolution of both (a, c) connectivity and (b, d) permeability with porosity for rocks from (a–b) effusive and (c–d) explosive eruptions. The upper and lower bounds on permeability are given (after Mueller et al., 2005) and are $k = 1 \times 10^{-17}\phi^{3.8}$ and $k = 1 \times 10^{-17}\phi^{3}$, respectively for rocks formed by effusive eruptions; or $k = 8 \times 10^{-15}(\phi - \phi_c)^2$ and $k = 1 \times 10^{-16}(\phi - \phi_c)^2$, respectively for rocks formed by explosive eruptions, where a common ϕ_c is estimated at 0.3 (Mueller et al., 2005). Microvesicular pumices from the Kos Plateau tuff (blue triangles; Bouvet de Maisonneuve et al., 2009) are differentiated from the other rhyolitic pumices (blue circles). The grey fields correspond to unphysical values of connectivity with $C > 1$. Details on compiled data are available in Supplementary Table 2. (For interpretation of the references to colour in this figure legend, the reader is referred to the web version of this article.)

proximately with $10^{-15} < k < 10^{-11}$ m^2 regardless of composition and no trend is observed (Fig. 3d). Note also that the majority of these vesicular rocks fall within the wide empirical bounds provided by Mueller et al. (2005) for explosive volcanic rocks for which $\phi_c \equiv 0.3$. If we instead compare how C varies with ϕ for these same data (Fig. 3c), basaltic, andesitic, trachytic and dacitic vesicular rocks cluster with moderate to high C, but the rhyolitic pumices demonstrate that low C is achieved at mid to high ϕ. This suggests that for some of the rhyolitic pumice suites $\phi_c > 0.3$. These observations are consistent with high experimentally determined ϕ_c for some vesiculating systems (Fig. 1) and with findings of other workers (Rust and Cashman, 2011 and references therein) and demonstrate that a universal ϕ_c constrained on the basis of k (Mueller et al., 2005) may not be appropriate.

Another important detail can be seen when considering the relationship between connectivity and permeability (Fig. 4). Conceptually, as $C \to 0$ at $\phi \to \phi_c$ permeability must also tend to zero. But as $C \to 1$ there is no strict limit on ϕ or k, both of which can increase while connectivity remains at unity. Therefore, C contains the most useful information about the evolution k in the region of $\phi \sim \phi_c$. This is demonstrated in Fig. 4 where we show that for all compositions there is a clustering of k values around $C = 1$ but a non-linear tail as we track from $C = 1$ down to $C < 1$. Unfortunately, there is little data in the region of low C for which permeability data also exist and as such we cannot observe the expected limit as C and k approach zero. It also appears that rocks formed in explosive eruptions have a generally higher k for a given C than rocks produced in effusive eruptions, which likely reflects fundamental differences in the pore geometries generally formed in those two eruption styles, as has been previously suggested (Mueller et al., 2005).

4. Extended discussion

4.1. Granular and non-granular materials: Insights from experimental work

We highlight that a subset of densification trends in Fig. 1 derive from initially granular materials, while the vesiculation trends are for non-granular porous media. Here we discuss the differences one might expect from this geometric distinction.

First, for the densification data presented in Fig. 1 (Robert et al., 2008; Vasseur et al., 2013, 2016), the evolution of C with ϕ appears to a first order to be independent of the densification mechanism over a wide range of conditions. For the data from Robert et al. (2008), granular volcanic ash was partially sintered before being drilled to a cylindrical core, then a uniaxial load was applied resulting in a range of strain rates at high temperature in the viscous regime such that densification proceeded before quenching. The data from Vasseur et al. (2013, 2016) were produced using granular crushed synthetic glass shards loaded in crucibles and densification proceeded under surface tension at the particle interfaces, no applied load was used. In Okumura et al. (2013), the densification arises from shear-induced outgassing of a highly connected pore network. In Kennedy et al. (2016), surface tension-driven retraction of bubble walls led to the densification of crystal-bearing pumices. Despite these large differences in densification mechanism, C and ϕ vary consistently such that we conclude that in the viscous regime densification trends produce a similar evolution of connectivity.

On the other hand, examination of the data for the vesiculation trend presented in Fig. 1 shows that the same mechanism-invariance of the trend of C with ϕ cannot hold here. As an example, the increase in C from ϕ_c occurs at a much lower window of

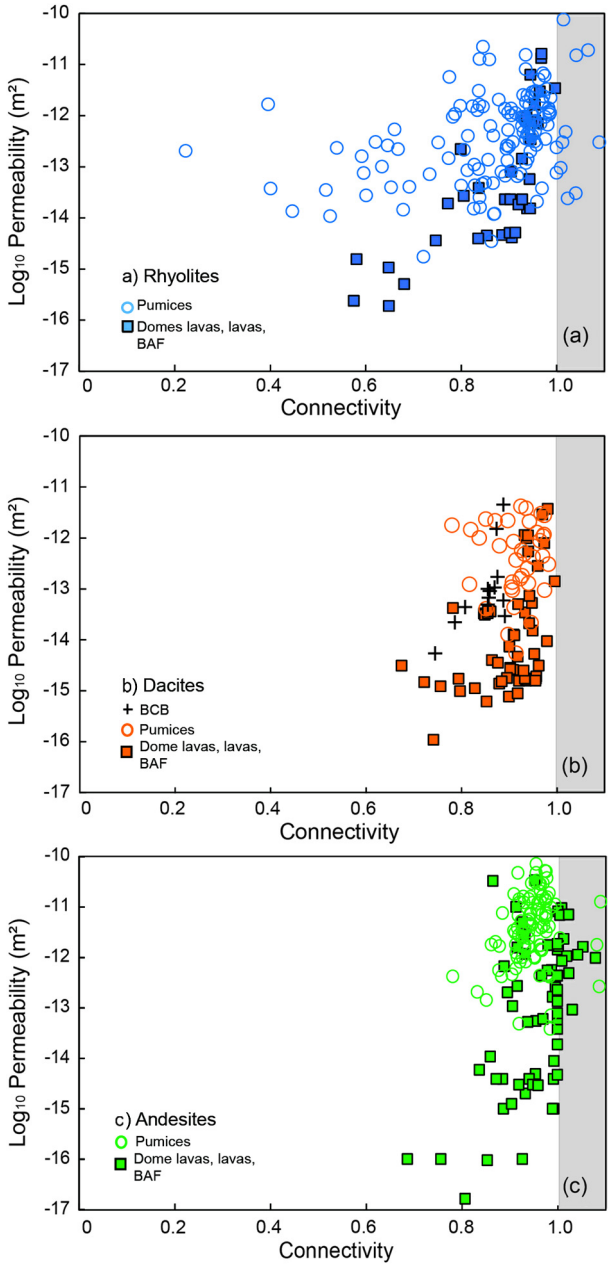

Fig. 4. The variation of connectivity C with permeability k for (a) rhyolites, (b) dacites, and (c) andesites, separated into classes of rocks produced in effusive activity and rocks produced in explosive activity. The grey fields correspond to unphysical values of connectivity with $C > 1$. BCB and BAF are breadcrust bombs and rocks from block and ash flow deposits, respectively. Details on compiled data are available in Supplementary Table 2.

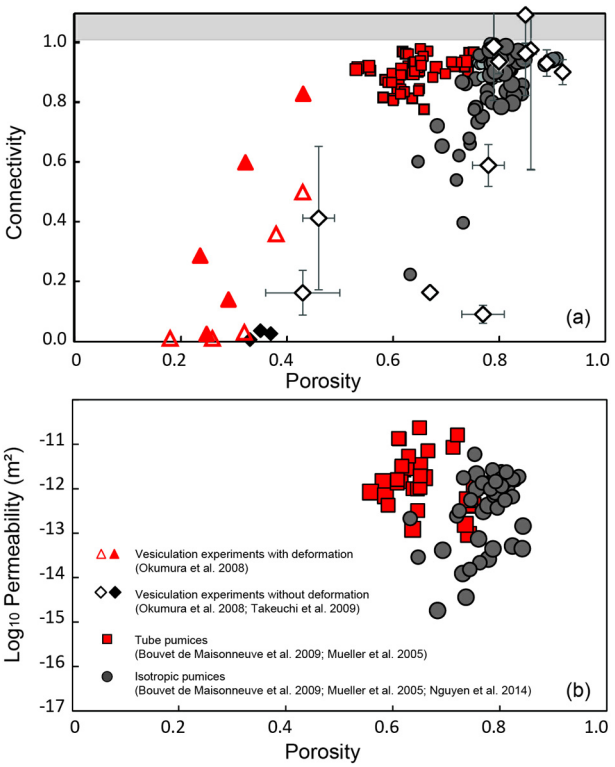

Fig. 5. Effect of shear-deformation on (a) the connectivity and (b) permeability with porosity for natural rhyolitic and dacitic pumices and experimental products. The grey field corresponds to unphysical values of connectivity with $C > 1$.

ϕ for experiments in which vesiculation was coincident with applied shear stress than for vesiculation experiments in the absence of shear stress (Okumura et al., 2008; Takeuchi et al., 2009). This indicates that bubble growth-driven coalescence is strongly influenced by shear strain whereas the deformation of initially granular materials is less influenced by deformation (Fig. 5).

4.2. The percolation threshold ϕ_c in magmas

In percolation theory, a common method for predicted ϕ_c is to create numerically generated porous networks from distributions of discs (2D) or spheres (3D). These are strictly geometrical, and not dynamic considerations of ϕ_c. These techniques predict that monodisperse spheres, distributed randomly in a volume where they can also overlap, achieve system-spanning connectivity at $\phi_c \sim 0.3$ when the spheres are considered to be the pore-phase (e.g., Rintoul, 2000). Treating the spheres as the pore phase in this way can be thought of as being most similar to the vesiculating case. Contrastingly, if the spheres are considered to be the non-pore phase (the solid in the case of rock or the liquid-crystal suspension in the case of magma), then ϕ_c is only recorded when the overlapping spheres occlude a system-spanning connection at much lower ϕ. Typically, in this case, $\phi_c \approx 0.03$ (Rintoul, 2000; Wadsworth et al., 2016a, 2016b). This second case, where the spheres are the non-pore matrix material is broadly analogous to the volcanic welding scenario. We find it informative to highlight how these ϕ_c constraints for sphere populations are altered by simple variables in both cases; (1) where the spheres are the pores and (2) where the spheres are particles. In case (1) ϕ_c is a strong function of the polydispersivity of the spheres sizes used in the geometrical simulation (e.g., Blower, 2001), whereas in case (2) ϕ_c is a weak function of polydispersivity (Rintoul, 2000). This is further demonstrated in Fig. 1, where ϕ_c covers a wide range of values for the vesiculating case (case 1), whereas ϕ_c is ubiquitously consistent with the $\phi_c = 0.03$ prediction for the granular case (case 2). Microvesicular rhyolitic pumices from the Kos Plateau tuff (Bouvet de Maisonneuve et al., 2009) contain two vesicle populations attributed to two distinct nucleation events. Consequently, these pumices apparently record a more complex approach to the percolation threshold (Fig. 3).

In natural magmas, the intersection of the percolation threshold as ϕ increases or decreases is often complicated by dynamic processes that may invalidate the numerical geometrical approaches outlined above. Some of these are discussed briefly here. Variable ϕ_c have been discussed in numerical, experimental or permeability studies (Rust and Cashman, 2011 and literature therein) with reference to dynamic scenarios. First, crystallinity has been shown to halt densification processes at a ϕ greater than ϕ_c that would

have been predicted on geometrical grounds alone, due to crystal–crystal interactions (Kennedy et al., 2016). These interactions produce a rigid framework and thus an elevated yield stress in the system that needs to be overcome for densification to proceed to ϕ_c. In some of these cases, however, the system is still percolating (i.e. permeable) even when changes in ϕ have stopped.

Additional, first-order effects controlling ϕ_c and the onset of connectivity for vesicular magmas are the presence or not of shear-deformation (Okumura et al., 2008; Takeuchi et al., 2009; Burgisser and Gardner, 2004; Rust and Cashman, 2011), the melt crystallinity and the modality of the vesicle size distribution in vesiculating systems (Blower, 2001). Shear-stress and the resulting deformation will favour the onset of connectivity and permeability at a lower ϕ_c as shown by decompression and vesiculation experiments (Figs. 1 and 5; Okumura et al., 2008, 2013; Takeuchi et al., 2009; Namiki and Manga, 2008). Tube pumices, generally the product of large shear strain (Dingwell et al., 2016), are consistent with experimental work for which vesiculation was coincident with shear deformation (Fig. 5). Contrastingly, isotropic pumice materials are more consistent with experiments where vesiculation happens in the absence of shear deformation (Figs. 1 and 5). It is clear from both natural and experimental datasets that ϕ_c is significantly reduced in the presence of shearing, consistent with previous studies (Okumura et al., 2008; Burgisser and Gardner, 2004).

The differences in ϕ_c between vesicular rocks might be also related to differences in crystallinity. The role of crystals on the connectivity and percolation threshold is complex. First, because bubbles cannot occupy the crystal-phase, for a given porosity, the addition of crystals reduces the space between bubbles, therefore enhancing coalescence at lower porosities (Blower, 2001). Second, the crystals are barriers to simple flow patterns and so they promote bubble deformation enhancing the likelihood of coalescence (Oppenheimer et al., 2015). In both cases, the addition of crystals appears to induce a shift of ϕ_c to lower porosity. Inversely, ϕ_c in crystal poor pumices might be quite high (Nakamura et al., 2008; Rust and Cashman, 2011). Even though our database lacks significant crystallinity data to establish definitive implications for the percolation threshold, we stress that rhyolitic pumices with a potentially high ϕ_c also have low melt crystallinity (<20 vol%; Bouvet de Maisonneuve et al., 2009; Alfano et al., 2012). Inversely, andesitic bread crust bombs have a very low percolation threshold associated with a high melt crystallinity of more than 50 vol% (Giachetti et al., 2010).

4.3. Distinguishing between eruptive styles

We propose that connectivity can be a useful tool to discriminate between different kinds of volcanic activity. The best example is the basaltic scoria from Hawaiian (fire fountaining) and Strombolian activity that have very distinct features when plotted together on a C–ϕ plot. Although these scoria have a similar porosity range, the scoria from fire fountaining have on average significantly lower and broader values of connectivity compared to scoria from Strombolian activity (Fig. 2b). The broad range of connectivity for scoria from fire fountaining can be interpreted simply by variations in time available before quenching due to differences in location and residence time in the fountain, as suggested by other authors for Hawaiian activity in Hawaii (Mangan and Cashman, 1996; Stovall et al., 2012); Etna (Polacci et al., 2006), Villarrica (Gurioli et al., 2008) and Al-Madinah, Saudi Arabia (Kawabata et al., 2015).

On the contrary, several factors can explain the higher connectivity observed for Strombolian activity such as higher average crystallinity, and more important degassing prior to the eruption. Note that the variations in time available before quenching are also observed for the connectivity of the breadcrust bombs (Fig. 1a) which is low in the rinds (fast quenching) and high in the cores (slow quenching).

4.4. The formation of effusive rocks: development of crack-networks and hysteresis

We can see from Figs. 2 and 3 that for the andesitic, dacitic and rhyolitic rocks produced in effusive eruptions, there is an apparently low ϕ_c that is inconsistent with experimental or numerical data for vesiculating systems and these data are not associated with samples that were initially granular. Therefore, we invoke here two possibilities for the additional mechanism that produces large C at low ϕ.

First, we propose that brittle deformation and the onset of crack network development can lead to this increase of C at low ϕ. This is consistent with experimental work that demonstrates that even small shear strain in high viscosity systems, such as andesitic to rhyolitic magmas, can result in brittle deformation (Lavallée et al., 2008; Cordonnier et al., 2009; Kendrick et al., 2013). This is an additional process that implicates potential variability in the value of ϕ_c. Most simply, cracks will form in magma when the product of the local shear strain rate $\dot{\varepsilon}$ and the liquid relaxation time λ, which is $\dot{\varepsilon}\lambda$, approaches unity (Dingwell and Webb, 1989). When the system only consists of liquid (pure melt) then this might occur as the bulk shear strain rate increases such that $\dot{\varepsilon}\lambda$ approaches 1. However, when the system suspends crystals, for example, the local strain rate is larger between the crystals, resulting in crack formation in the liquid when the bulk shear strain rate is $\dot{\varepsilon}\lambda < 1$. In this case, Cordonnier et al. (2012) showed that $\dot{\varepsilon}_c\lambda \propto 1 - (\phi_x/\phi_M)$ where $\dot{\varepsilon}_c$ is the bulk shear strain rate required to crack the liquid between the crystals, ϕ_x is the crystal volume fraction, and ϕ_M is the maximum packing of those crystals. Cracks additionally form as magmas cool. If cracks develop and span the system being measured, then C can increase to large values at low ϕ, even when ϕ is less than the predicted ϕ_c for that vesiculating system. If this is the mechanism that is driving the development of large C at anomalously low ϕ for the andesitic, dacitic and rhyolitic lavas presented in Figs. 2 and 3 then not only is crack development ubiquitous in these lava-forming systems, but also system-spanning crack development occurs while ϕ is low.

Another possible explanation is a cycle with (i) an early coalescence event increasing porosity and connectivity and the creation of a permeable pore space and (ii) gas escape through this permeable porous network leading to compaction and reduction of C and ϕ. During this compaction, cracks or crystals could act to maintain a relatively high connectivity (Kennedy et al., 2016). This succession of coalescence and gas escape would result in a hysteresis in the time-dependence of the relationship between C and ϕ. Okumura et al. (2013) experimentally obtained this type of hysteresis with an initial coalescence stage at a low ϕ_c by shearing followed by gas escape and compaction (Fig. 1).

These two possibilities are illustrated for rhyolites in Fig. 6 which is a conceptual drawing illustrating the temporal evolution of porosity and connectivity for different processes and showing the associated textures. The different connectivity paths in this conceptual model were constructed based on direct measurements or on constraints of the percolation threshold from experimental studies of vesiculation and densification of rhyolitic melts. The percolation threshold in the case of vesiculation in the absence of cracking and shear-deformation is typically high (path A–B in Fig. 6a; Takeuchi et al., 2009) and could occur in a wide range of porosity between 0.4 and the maximum face-centred cubic packing of bubbles of $\pi/3\sqrt{2} \approx 0.74$. In the case of vesiculation experiments in the presence of shearing (path C–E in Fig. 6a), the percolation threshold was significantly lower with $\phi_c \sim 0.2$ (Okumura et al., 2008) and the connectivity increases steeply with porosity.

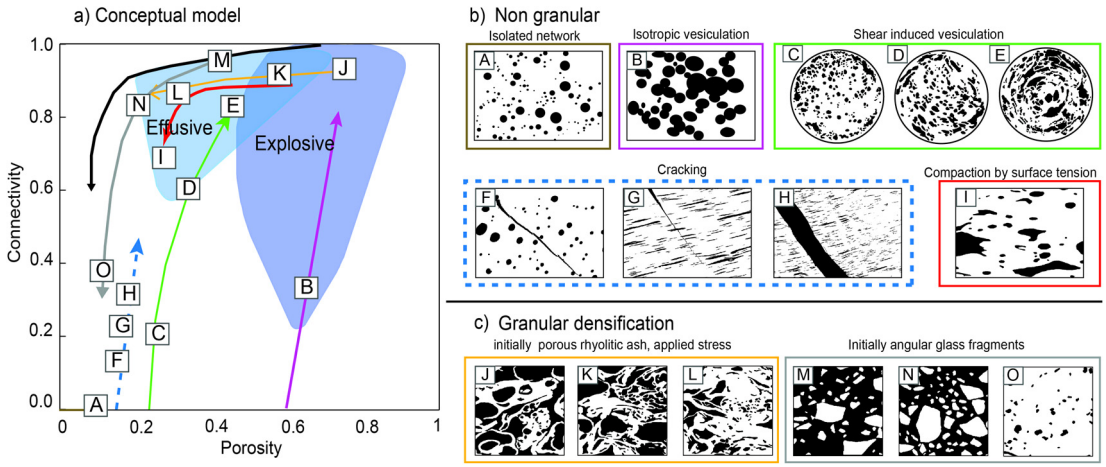

Fig. 6. Different paths of connectivity with porosity for different processes in rhyolitic magma. (a) The map of C with ϕ where the shaded areas for the rhyolitic rocks from effusive and those from explosive eruptions for reference (see Fig. 2) and the trends for cracking, vesiculation and densification of rhyolitic melts are reported. (b–c) Representative binary images of experimental samples produced under different conditions in (b) non-granular systems, and (c) granular systems. In all cases the black represents the pore phase. In (a), the lettered points refer to the images in (b) and (c) and appear at the respective measured ϕ and C. The path between the origin and point A represents the vesiculation of an isolated network of bubbles. The path through B represents vesiculation and coalescence without shear deformation (isotropic). The path C–E represents vesiculation in the presence of shear deformation (anisotropic; Okumura et al., 2008). The path F–G represents cracks connecting isolated, elongated bubbles with a percolation threshold at $\phi_c \sim 0.14$ (Kushnir et al., 2016). The path to point I is that for densification under surface tension of natural non-granular samples (Kennedy et al., 2016). The path J–L is the representation of viscous sintering of porous rhyolitic ash under compactive applied stress (Robert et al., 2008). Path M–O is for viscous sintering of glass fragments under surface tension (Vasseur et al., 2016). The dashed line corresponds to the path F–G for which there are no direct measurements of connectivity and was drawn from the experimental constraints on the initial porosity and the percolation threshold only (Kushnir et al., 2016). Otherwise paths are drawn connecting measured data points. The dark solid line corresponds to the trend of compaction by gas escape after initial vesiculation in the presence of shear-deformation (Okumura et al., 2013).

The percolation threshold in the presence of cracks can be even lower and the connectivity can increase dramatically with only minor changes in porosity. In the case presented here (paths F–G–H in Fig. 6a), cracks connect a population of initially isolated, elongated bubbles formed in torsion experiments on bubble-bearing silicate melts (Kushnir et al., 2016). In this case, the initial porosity before the crack formation was approximately $\phi \sim 0.14$ and the percolation threshold must therefore also be $\phi_c \sim 0.14$. Textures similar to those of these experiments can be observed in dense effusive rhyolites from a rhyolitic dome at Novarupta volcano (Adams et al., 2006; Nguyen et al., 2014). All of these cracking and vesiculation processes could be followed by densification due to gas escape leading to a hysteresis. The path terminating at L (Fig. 6a) represents a densification by gas escape process following a vesiculation event (Okumura et al., 2013). In this case, the outgassing was accompanied by shearing and compaction. In the case of gas escape under surface tension (Kennedy et al., 2016), the densification can reduce significantly connectivity at a high porosity (path terminating at I in Fig. 6a). We also include in Fig. 6 the case of granular densification by welding of porous rhyolitic ash under compaction (path J–L; Robert et al., 2008) and sintering of dense angular glass fragments (path M–O; Vasseur et al., 2016), that lead to reduction of porosity and connectivity. This process is important in tuffisite veins and could be implicated in the formation of effusive lavas that represent densified pyroclastic material (e.g., Castro et al., 2014). This model implies that information about the texture of a rhyolite can provide insights into the connectivity path and associated dominant process. However, most of these possible paths cross the field of measured ϕ and C values for effusive rocks and similar textures could be observed for rocks formed in different processes making interpretations difficult unless samples with a range of ϕ are collected that can be attributed to a single mechanism. Furthermore, it must be noted that other cracking, vesiculation and densification paths are possible but we only reported here the trends constrained by experimental studies to compare with the range of natural data.

5. Conclusions

We present here a database of pore connectivity C and porosity ϕ data for natural volcanic rocks ($n = 2715$) and experimental products ($n = 116$) from published sources and additional measurements. When available, permeability data was also included for comparison ($n = 535$). Analysis of these data lead to the following broad conclusions:

- Connectivity can be used to distinguish between subsets of volcanic materials including effusive and explosive products, products of fire fountaining and Strombolian basaltic activity and bulk chemical differences, when large datasets are measured or compiled.
- Connectivity can be used to identify the percolation threshold porosity as it can be constrained in samples below and above this threshold, where permeability cannot.
- Pore connectivity develops by vesiculation and bubble growth-driven coalescence or by cracking or combinations of both processes. Pore connectivity decreases by densification processes including compaction, sintering or welding. The trend of connectivity with porosity is distinct for these porosity-increasing and porosity-decreasing processes.
- Connectivity potentially contains important information about permeability at porosities close to the percolation threshold where $0 < C < 1$.

Our work shows that a valuable frontier to pursue would be the systematic measurement of suites of rocks or experimental samples in the range where connectivity is less than unity but greater than zero. It is in this range that the co-variation of connectivity with porosity is directly informative of the evolution of permeability. That is, near to the percolation threshold, connectivity is an underutilized metric. Specifically this constraint for a range of processes could be achieved using tomographic techniques and targeted experimental work spanning the evolution from non-percolating to percolating systems during both vesiculation and densification processes. Key first order implications of

such constraints would be associated with knowing how and when permeability is established or shuts off in volcanic interiors or deposits. In turn, this would permit us to know under what conditions a volcano may start to build fluid overpressure leading to an eruption and when the volcano may effectively dissipate overpressure.

Acknowledgements

B.S. and M.C. acknowledge the PROCOPE grant (grant no. 57130387), funded and implemented by the Deutscher Akademischer Austauschdienst (DAAD) in Germany, and the Ministry of Foreign and European Affairs (MAE) and the Ministry of Higher Education and Research (MENESR) in France. D.B.D. acknowledges the support of the ERC Advanced Grant (EVOKES — no. 247076). This research was partially financed by the French Government Laboratory of Excellence (initiative no. ANR-10-LABX-0006), the Région Auvergne, and the European Regional Development Fund. Work was also supported by the Laboratory of Excellence ClerVolc (contribution number 236). We also thank the editor Tamsin Mather who helped to reinforce the clarity and implications of the manuscript. This paper has benefited from constructive reviews by two anonymous reviewers. We thank H.M.N. Wright, J. Vasseur, K.J. Russel, S.J. Cronin, F. Alfano and T. Platz for providing raw data. We are thankful to Jérémie Vasseur for the helpful discussions.

Appendix A. Supplementary material

Supplementary material related to this article can be found online at http://dx.doi.org/10.1016/j.epsl.2017.01.011.

References

Adams, N.K., Houghton, B.F., Fagents, S.A., Hildreth, W., 2006. The transition from explosive to effusive eruptive regime: the example of the 1912 Novarupta eruption, Alaska. Bull. Geol. Soc. Am. 118, 620–634. http://dx.doi.org/10.1130/B25768.1.

Alfano, F., Bonadonna, C., Gurioli, L., 2012. Insights into eruption dynamics from textural analysis: the case of the May, 2008, Chaitén eruption. Bull. Volcanol. 74, 2095–2108. http://dx.doi.org/10.1007/s00445-012-0648-3.

Bernard, M.L., Zamora, M., Géraud, Y., Boudon, G., 2007. Transport properties of pyroclastic rocks from Montagne Pelée volcano (Martinique, Lesser Antilles). J. Geophys. Res., Solid Earth 112, 1–16. http://dx.doi.org/10.1029/2006JB004385.

Blower, J., 2001. Factors controlling permeability–porosity relationships in magma. Bull. Volcanol. 63, 497–504. http://dx.doi.org/10.1007/s004450100172.

Bouvet de Maisonneuve, C., Bachmann, O., Burgisser, A., 2009. Characterization of juvenile pyroclasts from the Kos Plateau Tuff (Aegean Arc): insights into the eruptive dynamics of a large rhyolitic eruption. Bull. Volcanol. 71, 643–658. http://dx.doi.org/10.1007/s00445-008-0250-x.

Burgisser, A., Gardner, J.E., 2004. Experimental constraints on degassing and permeability in volcanic conduit flow. Bull. Volcanol. 67, 42–56. http://dx.doi.org/10.1007/s00445-004-0359-5.

Calder, E.S., et al., 2015. Lava dome eruptions. In: Encyclopedia of Volcanoes, 2nd ed. Academic Press, San Diego.

Castro, J.M., Cordonnier, B., Tuffen, H., Tobin, M.J., Puskar, L., Martin, M.C., Bechtel, H.A., 2012. The role of melt-fracture degassing in defusing explosive rhyolite eruptions at volcán Chaitén. Earth Planet. Sci. Lett. 333–334, 63–69. http://dx.doi.org/10.1016/j.epsl.2012.04.024.

Castro, J.M., Bindeman, I.N., Tuffen, H., Ian Schipper, C., 2014. Explosive origin of silicic lava: textural and δD–H_2O evidence for pyroclastic degassing during rhyolite effusion. Earth Planet. Sci. Lett. 405, 52–61. http://dx.doi.org/10.1016/j.epsl.2014.08.012.

Colombier, M., Gurioli, L., Druitt, T.H., Shea, T., Boivin, P., Miallier, D., Cluzel, N., 2017. Textural evolution of magma during the 9.4 ka trachytic explosive eruption at Kilian Volcano, Chaîne des Puys, France. Bull. Volcanol. 79, 17. http://dx.doi.org/10.1007/s00445-017-1099-7.

Connor, C.B., Lichtner, P.C., Conway, F.M., Hill, B.E., Ovsyannikov, A.A., Federchenko, I., Doubik, Y., Shapar, N., Taran, Y.A., Lichtner, P.C., 1997. Cooling of an igneous dike 20 yr after intrusion. Geology 25 (8), 711–714. http://dx.doi.org/10.1130/0091-7613(1997)025<0711.

Cordonnier, B., Hess, K., Lavallee, Y., Dingwell, D.B., 2009. Rheological properties of dome lavas: case study of Unzen volcano. Earth Planet. Sci. Lett. 279, 263–272. http://dx.doi.org/10.1016/j.epsl.2009.01.014.

Cordonnier, B., Caricchi, L., Pistone, M., Castro, J., Hess, K., Gottschaller, S., Manga, M., Dingwell, D.B., 2012. The viscous-brittle transition of crystal-bearing silicic melt: direct observation of magma rupture and healing. Geology, 5–8. http://dx.doi.org/10.1130/G3914.1.

Degruyter, W., Burgisser, A., Bachmann, O., Malaspinas, O., 2010. Synchrotron X-ray microtomography and lattice Boltzmann simulations of gas flow through volcanic pumices. Geosphere 6, 470–481. http://dx.doi.org/10.1130/GES00555.1.

Dingwell, D.B., Webb, S.L., 1989. Structural relaxation in silicate melts and non-Newtonian melt rheology in geologic processes. Phys. Chem. Miner. 16 (5), 508–516.

Dingwell, D.B., Lavallée, Y., Hess, K., Flaws, A., Marti, J., Nichols, A.R.L., Gilg, H.A., Schillinger, B., 2016. Eruptive shearing of tube pumice: pure and simple. Solid Earth 7, 1383–1393. http://dx.doi.org/10.5194/se-7-1383-2016.

Edmonds, M., Herd, R.A., 2007. A volcanic degassing event at the explosive–effusive transition. Geophys. Res. Lett. 34, 1–6. http://dx.doi.org/10.1029/2007GL031379.

Eichelberger, J.C., Carrigan, C.R., Westrich, H.R., Price, R.H., 1986. Non-explosive silicic volcanism. Nature 323 (6089), 598–602.

Farquharson, J., Heap, M.J., Varley, N.R., Baud, P., Reuschlé, T., 2015. Permeability and porosity relationships of edifice-forming andesites: a combined field and laboratory study. J. Volcanol. Geotherm. Res. 297, 52–68. http://dx.doi.org/10.1016/j.jvolgeores.2015.03.016.

Formenti, Y., Druitt, T.H., 2003. Vesicle connectivity in pyroclasts and implications for the fluidisation of fountain-collapse pyroclastic flows, Montserrat (West Indies). Earth Planet. Sci. Lett. 214, 561–574. http://dx.doi.org/10.1016/S0012-821X(03)00386-8.

Giachetti, T., Druitt, T.H., Burgisser, A., Arbaret, L., Galven, C., 2010. Bubble nucleation, growth and coalescence during the 1997 vulcanian explosions of Soufrière Hills Volcano, Montserrat. J. Volcanol. Geotherm. Res. 193, 215–231. http://dx.doi.org/10.1016/j.jvolgeores.2010.04.001.

Gonnermann, H.M., Manga, M., 2003. Explosive volcanism may not be an inevitable consequence of magma fragmentation. Nature 426, 8–11. http://dx.doi.org/10.1038/nature02159.1.

Gonnermann, H.M., Manga, M., 2007. The fluid mechanics inside a volcano. http://dx.doi.org/10.1146/annurev.fluid.39.050905.110207.

Gonnermann, H.M., Manga, M., 2012. Dynamics of magma ascent in the volcanic conduit. In: Modeling Volcanic Processes: The Physics and Mathematics of Volcanism. Cambridge University Press, pp. 55–84.

Gurioli, L., Harris, A.J.L., Houghton, B.F., Polacci, M., Ripepe, M., 2008. Textural and geophysical characterization of explosive basaltic activity at Villarrica volcano. J. Geophys. Res. 113, 1–16. http://dx.doi.org/10.1029/2007JB005328.

Heap, M.J., Farquharson, J.I., Wadsworth, F.B., Kolzenburg, S., Russell, J.K., 2015. Timescales for permeability reduction and strength recovery in densifying magma. Earth Planet. Sci. Lett. 429, 223–233. http://dx.doi.org/10.1016/j.epsl.2015.07.053.

Kato, Y., 1987. Woody pumice generated with submarine eruption. Chishitsugaku Zasshi 93, 11–20.

Kawabata, E., Cronin, S.J., Bebbington, M.S., Moufti, M.R.H., El-Masry, N., Wang, T., 2015. Identifying multiple eruption phases from a compound tephra blanket: an example of the AD1256 Al-Madinah eruption, Saudi Arabia. Bull. Volcanol. 77. http://dx.doi.org/10.1007/s00445-014-0890-y.

Kendrick, J.E., Lavallée, Y., Hess, K., Heap, M.J., Gaunt, H.E., Meredith, P.G., Dingwell, D.B., 2013. Tracking the permeable porous network during strain-dependent magmatic flow. J. Volcanol. Geotherm. Res. 260, 117–126. http://dx.doi.org/10.1016/j.jvolgeores.2013.05.012.

Kendrick, J.E., Lavallée, Y., Varley, N.R., Wadsworth, F.B., Lamb, O.D., Vasseur, J., 2016. Blowing off steam: tuffisite formation as a regulator for lava dome eruptions. Front. Earth Sci. 4, 1–15. http://dx.doi.org/10.3389/feart.2016.00041.

Kennedy, B.M., Jellinek, A.M., Russell, J.K., Nichols, A.R.L., Vigouroux, N., 2010. Time- and temperature-dependent conduit wall porosity: a key control on degassing and explosivity at Tarawera volcano, New Zealand. Earth Planet. Sci. Lett. 299, 126–137. http://dx.doi.org/10.1016/j.epsl.2010.08.028.

Kennedy, B.M., Wadsworth, F.B., Vasseur, J., Schipper, C.I., Jellinek, A.M., Von Aulock, F.W., Hess, K., Russell, J.K., Lavallée, Y., Nichols, A.R.L., Dingwell, D.B., 2016. Surface tension driven processes densify and retain permeability in magma and lava. Earth Planet. Sci. Lett. 433, 116–124. http://dx.doi.org/10.1016/j.epsl.2015.10.031.

Klug, C., Cashman, K.V., 1996. Permeability development in vesiculating magmas: implications for fragmentation. Bull. Volcanol. 58, 87–100.

Klug, C., Cashman, K., Bacon, C., 2002. Structure and physical characteristics of pumice from the climactic eruption of Mount Mazama (Crater Lake), Oregon. Bull. Volcanol. 64, 486–501. http://dx.doi.org/10.1007/s00445-002-0230-5.

Kushnir, A.R.L., Martel, C., Bourdier, J., Heap, M.J., Reuschlé, T., Erdmann, S., Komorowski, J., Cholik, N., 2016. Probing permeability and microstructure: unravelling the role of a low-permeability dome on the explosivity of Merapi (Indonesia). J. Volcanol. Geotherm. Res. 316, 56–71. http://dx.doi.org/10.1016/j.jvolgeores.2016.02.012.

Lavallée, Y., Meredith, P.G., Dingwell, D.B., Hess, K., Wassermann, J., Cordonnier, B., Gerik, A., Kruhl, J.H., 2008. Seismogenic lavas and explosive eruption forecasting. Nature 453, 507–510. http://dx.doi.org/10.1038/nature06980.

Le Pennec, J.L., Hermitte, D., Isya, D., Pezard, P., Coulon, C., Cochemé, J.-J., Mulyadi, E., Ollagnier, F., Revest, C., 2001. Electrical conductivity and pore-space topology

of Merapi lavas: implication for the degassing of porphyritic andesite magmas. Geophys. Res. Lett. 28 (22), 4283–4286.

Lindquist, W.B., Lee, S.-M., Coker, D.A., Jones, K.W., Spanne, P., 1996. Medial axis analysis of void structure in three-dimensional tomographic images of porous media. J. Geophys. Res. 101, 8297. http://dx.doi.org/10.1029/95JB03039.

Mangan, M.T., Cashman, K.V., 1996. The structure of basaltic scoria and reticulite and inferences for vesiculation, foam formation, and fragmentation in lava fountains. J. Volcanol. Geotherm. Res. 0273, 1–18.

Michaut, C., Bercovici, D., Sparks, R.S.J., 2009. Ascent and compaction of gas rich magma and the effects of hysteretic permeability. Earth Planet. Sci. Lett. 282, 258–267. http://dx.doi.org/10.1016/j.epsl.2009.03.026.

Michol, K.A., Russell, J.K., Andrews, G.D.M., 2008. Welded block and ash flow deposits from Mount Meager, British Columbia, Canada. J. Volcanol. Geotherm. Res. 169, 121–144. http://dx.doi.org/10.1016/j.jvolgeores.2007.08.010.

Morandi, A., Di Muro, A., Principe, C., Michon, L., Leroi, G., Norelli, F., Bachèlery, P., 2016. Pre-historic (<5 kiloyear) explosive activity at Piton de la Fournaise volcano. In: Active Volcanoes of the Southwest Indian Ocean. Springer, Berlin, Heidelberg, pp. 107–138.

Mueller, S., 2007. Permeability and Porosity as Constraints on the Explosive Eruption of Magma: Laboratory Experiments and Field Investigations. PhD thesis.

Mueller, S., Melnik, O., Spieler, O., Scheu, B., Dingwell, D.B., 2005. Permeability and degassing of dome lavas undergoing rapid decompression: an experimental determination. Bull. Volcanol. 67, 526–538. http://dx.doi.org/10.1007/s00445-004-0392-4.

Mueller, S., Scheu, B., Spieler, O., Dingwell, D.B., 2008. Permeability control on magma fragmentation. Geology 36, 399–402. http://dx.doi.org/10.1130/G24605A.1.

Nakamura, M., Otaki, K., Takeuchi, S., 2008. Permeability and pore-connectivity variation of pumices from a single pyroclastic flow eruption: implications for partial fragmentation. J. Volcanol. Geotherm. Res. 176, 302–314. http://dx.doi.org/10.1016/j.jvolgeores.2008.04.011.

Namiki, A., Manga, M., 2008. Transition between fragmentation and permeable outgassing of low viscosity magmas. J. Volcanol. Geotherm. Res. 169, 48–60. http://dx.doi.org/10.1016/j.jvolgeores.2007.07.020.

Nguyen, C.T., Gonnermann, H.M., Houghton, B.F., 2014. Explosive to effusive transition during the largest volcanic eruption of the 20th century (Novarupta 1912, Alaska). Geology 42, 703–706. http://dx.doi.org/10.1130/G35593.1.

Okumura, S., Nakamura, M., Tsuchiyama, A., Nakano, T., Uesugi, K., 2008. Evolution of bubble microstructure in sheared rhyolite: formation of a channel-like bubble network. J. Geophys. Res., Solid Earth 113, 1–18. http://dx.doi.org/10.1029/2007JB005362.

Okumura, S., Nakamura, M., Uesugi, K., Nakano, T., Fujioka, T., 2013. Coupled effect of magma degassing and rheology on silicic volcanism. Earth Planet. Sci. Lett. 362, 163–170. http://dx.doi.org/10.1016/j.epsl.2012.11.056.

Oppenheimer, J., Rust, A.C., Cashman, K.V., Sandnes, B., 2015. Gas migration regimes and outgassing in particle-rich suspensions. Front. Phys. 3, 1–13. http://dx.doi.org/10.3389/fphy.2015.00060.

Platz, T., Cronin, S.J., Cashman, K.V., Stewart, R.B., Smith, I.E.M., 2007. Transition from effusive to explosive phases in andesite eruptions – a case-study from the AD1655 eruption of Mt. Taranaki, New Zealand. J. Volcanol. Geotherm. Res. 161, 15–34. http://dx.doi.org/10.1016/j.jvolgeores.2006.11.005.

Polacci, M., Baker, D.R., Mancini, L., Tromba, G., Zanini, F., 2006. Three-dimensional investigation of volcanic textures by X-ray microtomography and implications for conduit processes. Geophys. Res. Lett. 33, 3–7. http://dx.doi.org/10.1029/2006GL026241.

Rintoul, M.D., 2000. Precise determination of the void percolation threshold for two distributions of overlapping spheres. Phys. Rev. E 62 (1), 68.

Robert, G., Russell, J.K., Giordano, D., 2008. Rheology of porous volcanic materials: high-temperature experimentation under controlled water pressure. Chem. Geol. 256, 215–229. http://dx.doi.org/10.1016/j.chemgeo.2008.06.028.

Rust, A.C., Cashman, K.V., 2004. Permeability of vesicular silicic magma: inertial and hysteresis effects. Earth Planet. Sci. Lett. 228, 93–107. http://dx.doi.org/10.1016/j.epsl.2004.09.025.

Rust, A.C., Cashman, K.V., 2011. Permeability controls on expansion and size distributions of pyroclasts. J. Geophys. Res., Solid Earth 116, 1–17. http://dx.doi.org/10.1029/2011JB008494.

Rust, A.C., Russell, J.K., Knight, R.J., 1999. Dielectric constant as a predictor of porosity in dry volcanic rocks. J. Volcanol. Geotherm. Res. 91, 79–96. http://dx.doi.org/10.1016/S0377-0273(99)00055-4.

Saar, M.O., Manga, M., 1999. Permeability–porosity relationship in vesicular basalts. Geophys. Res. Lett. 26 (1), 111–114.

Shea, T., Gurioli, L., Houghton, B.F., 2012. Transitions between fall phases and pyroclastic density currents during the AD 79 eruption at Vesuvius: building a transient conduit model from the textural and volatile record. Bull. Volcanol. 74, 2363–2381. http://dx.doi.org/10.1007/s00445-012-0668-z.

Shimano, T., Nakada, S., 2006. Vesiculation path of ascending magma in the 1983 and the 2000 eruptions of Miyakejima volcano, Japan. Bull. Volcanol. 68, 549–566. http://dx.doi.org/10.1007/s00445-005-0029-2.

Song, S.R., Jones, K.W., Lindquist, W.B., Dowd, B.A., Sahagian, D.L., 2001. Synchrotron X-ray computed microtomography: studies on vesiculated basaltic rocks. Bull. Volcanol. 63, 252–263. http://dx.doi.org/10.1007/s004450100141.

Stovall, W.K., Houghton, B.F., Hammer, J.E., Fagents, S.A., Swanson, D.A., 2012. Vesiculation of high fountaining Hawaiian eruptions: episodes 15 and 16 of 1959 Kīlauea Iki. Bull. Volcanol., 441–455. http://dx.doi.org/10.1007/s00445-011-0531-7.

Takeuchi, S., Tomiya, A., Shinohara, H., 2009. Degassing conditions for permeable silicic magmas: implications from decompression experiments with constant rates. Earth Planet. Sci. Lett. 283, 101–110. http://dx.doi.org/10.1016/j.epsl.2009.04.001.

Vasseur, J., Wadsworth, F.B., Lavallée, Y., Hess, K.U., Dingwell, D.B., 2013. Volcanic sintering: timescales of viscous densification and strength recovery. Geophys. Res. Lett. 40, 5658–5664. http://dx.doi.org/10.1002/2013GL058105.

Vasseur, J., Wadsworth, F.B., Lavallée, Y., Dingwell, D.B., 2016. Dynamic elastic moduli during isotropic densification of initially granular media. Geophys. J. Int. 204, 1721–1728. http://dx.doi.org/10.1093/gji/ggv550.

Vogel, H.-J., 2002. Topological characterization of porous media. In: Morphology of Condensed Matter. In: Lecture Notes in Physics, vol. 600, pp. 75–92.

Wadsworth, F.B., Vasseur, J., Von Aulock, F.W., Hess, K.-U., Scheu, B., Lavallée, Y., Dingwell, D.B., 2014. Nonisothermal viscous sintering of volcanic ash. J. Geophys. Res., Solid Earth. http://dx.doi.org/10.1002/2014JB011453.

Wadsworth, F.B., Vasseur, J., Llewellin, E.W., Schauroth, J., Dobson, K.J., Scheu, B., Dingwell, D.B., 2016a. Sintering of viscous droplets under surface tension. Proc. R. Soc. A 472 (2188), 20150780.

Wadsworth, F.B., Vasseur, J., Scheu, B., Kendrick, J.E., Lavallée, Y., Dingwell, D.B., 2016b. Universal scaling of fluid permeability during volcanic welding and sediment diagenesis. Geology 44, 219–222. http://dx.doi.org/10.1130/G37559.1.

Wright, H.M., Cashman, K.V., 2014. Compaction and gas loss in welded pyroclastic deposits as revealed by porosity, permeability, and electrical conductivity measurements of the Shevlin Park Tuff. Geol. Soc. Am. Bull. 126, 234–247. http://dx.doi.org/10.1130/b30668.1.

Wright, H.M.N., Cashman, K.V., Rosi, M., Cioni, R., 2007. Breadcrust bombs as indicators of vulcanian eruption dynamics at Guagua Pichincha volcano, Ecuador. Bull. Volcanol. 69, 281–300. http://dx.doi.org/10.1007/s00445-006-0073-6.

Wright, H.M.N., Cashman, K.V., Gottesfeld, E.H., Roberts, J.J., 2009. Pore structure of volcanic clasts: measurements of permeability and electrical conductivity. Earth Planet. Sci. Lett. 280, 93–104. http://dx.doi.org/10.1016/j.epsl.2009.01.023.

Yokoyama, T., Takeuchi, S., 2009. Porosimetry of vesicular volcanic products by a water-expulsion method and the relationship of pore characteristics to permeability. J. Geophys. Res., Solid Earth 114. http://dx.doi.org/10.1029/2008JB005758.